INSTITUTE OF PHYSICS PUBLISHING JOURNAL OF PHYSICS B: ATOMIC, MOLECULAR AND OPTICAL PHYSICS

J. Phys. B: At. Mol. Opt. Phys. **36** (2003) 4813–4826 PII: S0953-4075(03)66932-4

H_2 dissociation by H^+ and He^{2+} projectiles at intermediate energies

S Martínez, G Bernardi, P Focke, A D González and S Suárez

Centro Atómico Bariloche and Instituto Balseiro[1], 8400 S C de Bariloche, Río Negro, Argentina

E-mail: smartine@cab.cnea.gov.ar

Received 28 July 2003
Published 21 November 2003
Online at stacks.iop.org/JPhysB/36/4813

Abstract

We have investigated proton emission from dissociated H_2 molecules after colliding with H^+ and He^{2+} ions with energies 25, 50 and 100 keV amu^{-1}. The energy spectra of protons have been obtained covering the angular range from 10° to 170° and fragment energies from 3–15 eV for He^{2+} projectiles and in the 0–15 eV range for H^+ impact, respectively. Using the Franck–Condon approximation we were able to find the relative contributions for some dissociation channels ($2p\pi_u$, $2s\sigma_g$, $2p\sigma_u$ and Coulomb explosion (CE)). For He^{2+} projectiles we found that the momentum transfer to the target must be included in the model to obtain a better description of the experimental results. When compared to the H^+ impact case, we observe for He^{2+} projectiles the enhancement of the CE channel due to higher capture probabilities. Differential cross sections as a function of emission angle were obtained to investigate the orientation dependence of the electronic processes leading to dissociation. Total cross sections are also estimated and compared to measurements from other laboratories.

1. Introduction

The dissociation of molecular species resulting after the interaction with photons, electrons and ions has been the subject of study by several research groups (Latimer 1993 and references therein). Increasing activity in the study of the dissociation of complex molecules has been observed over the last few years, mainly of those of interest in the atmospheric, biological and other fields. Nevertheless, simple diatomic molecules remain as test cases in discussing such many-body processes. Detailed experimental information, besides total cross sections for the different dissociation channels, can be obtained from the measurement of energy and angular distributions of fragments. Under certain assumptions, the angular distributions allow us to also study the dependence of collision processes with respect to the spatial orientation of the

[1] Comisión Nacional de Energía Atómica and Universidad Nacional de Cuyo, Argentina.

internuclear axis of the molecule. In the present work we use the simplest neutral molecule, H_2, taking advantage of well known potential curves and, by using bare ion projectiles, we deal only with two electrons involved in the collision-induced fragmentation process.

Excluding ground state dissociation (GSD) of H_2^+ after one-electron ionization of H_2, $H_2^+(1s\sigma_g) \rightarrow H^+ + H^0(1s)$, the fragmentation of H_2 by a bare A^{Z+} projectile arises from two-electron processes (Ben-Itzhak *et al* 1996). These are

$$A^{Z+} + H_2 \rightarrow \begin{cases} A^{(Z-2)+} + 2H^+ & \text{double capture (DC)} \\ A^{(Z-1)+} + 2H^+ + e^- & \text{transfer ionization (TI)} \\ A^{Z+} + 2H^+ + 2e^- & \text{double ionization (DI),} \end{cases}$$

which lead to the so-called Coulomb explosion (CE) of the two remaining protons and

$$A^{Z+} + H_2 \rightarrow \begin{cases} A^{(Z-1)+} + H_2^{+*} & \\ A^{(Z-1)+} + H^+ + H_0 & \text{transfer excitation (TE)} \\ A^{Z+} + H_2^{+*} + e^- & \\ A^{Z+} + H^+ + H^0 + e^- & \text{ionization excitation (IE)} \\ A^{Z+} + H_2^{**} & \\ A^{Z+} + H^+ + H^0 + e^- & \text{autoionization (AI)} \\ A^{Z+} + H^0 + H^0 & \text{neutral dissociation.} \end{cases}$$

The main features of the proton spectra from dissociation of H_2, i.e. dissociative states involved, angular distributions, transfer of momentum, thermal broadening and thresholds, were first observed in the electron impact case (Dunn and Kieffer 1963, Zare 1967, Köllman 1978, Burrows *et al* 1980, Landau *et al* 1981). Similar studies were also performed for photon impact, although recent efforts were directed mainly at identifying the doubly excited states and fragment production (Strathdee and Browning 1979, Latimer *et al* 1993, Ito *et al* 1996, Sánchez and Martín 1999).

In fast ion impact dissociation of H_2, Edwards, Wood and co-workers have done comparative studies with 0.35–3.5 MeV amu^{-1} protons and equivelocity electrons (Edwards *et al* 1990, 1992). These authors have measured proton spectra for emission angles from 18° up to 90°, from which total and angular cross sections were obtained for the different dissociation channels, as well as the contribution from AI to proton production. Latimer and co-workers have studied fragment and pair proton production for 3–30 keV H^+ and He^+ projectile beams (Lindsay *et al* 1987, Savage *et al* 1990), measuring energy spectra for emission angles in the range 30°–150°. Yousif *et al* (1988) proved the usefulness of the Franck–Condon approximation in the analysis of proton pair production in order to obtain the vibrational ground state of H_2. The development of the momentum imaging technique using position-sensitive detectors (Ali *et al* 1999, Dörner *et al* 2000) has provided detailed information on molecular recoil ions and ionized electrons in dissociation collision measurements. Ali *et al* (2001) performed a kinematically complete study in double capture for 50 keV H^+ and 0.2–10 keV amu^{-1} Xe^{26+} on D_2. Ben-Itzhak *et al* (1996) investigated the contribution of GSD to total proton production and found a theoretical value of 1.5% for the fraction of H_2^+ dissociated through this mechanism. They confirmed the validity of this finding by experimental results for a projectile velocity range $v_P = 6$–24 au. GSD was also comparatively investigated for H_2^+ and D_2^+ after ionizing collisions and electron capture by He^+ at $v_P = 0.25$ and 0.5 au (Wolff *et al* 2002).

In the present work we report experimental results for H^+ and He^{2+} projectiles incident on H_2 at intermediate impact energies $E_P = 25$–100 keV amu^{-1}. Target dissociation was investigated by measuring energy spectra of protons at different emission angles, with respect to the ion beam direction, then evaluated by a fitting procedure considering three repulsive states

of H_2^+ ($2p\pi_u$, $2s\sigma_g$ and $2p\sigma_u$) and the pure Coulomb (H^+H^+) potential channel. The analysis of the data is based on the Franck–Condon approximation, which was successfully applied to H_2 dissociation for impact energies below 30 keV amu^{-1} and greater than 350 keV amu^{-1} (Wood *et al* 1977, Lindsay *et al* 1987, Yousif *et al* 1988). In the present measurements we do not detect the charge state of the outgoing projectiles, though it is known that at the lowest measured energy (25 keV amu^{-1}) electron capture prevails, while at 100 keV amu^{-1} there is an increasing contribution from pure ionization, i.e. electron emission not associated with charge exchange.

2. Experimental procedure

The measurements were performed with the experimental set-up described previously (Bernardi *et al* 1996). Minor modifications in order to measure positively charged particles instead of electronic spectra were made. In brief, H^+ and $^3He^{2+}$ beams from the ion accelerator were energy analysed by a 90° deflection magnet and then collimated to 0.6×0.6 mm^2 by means of two sets of slits, before entering the collision chamber. The target is of the effusive type from an aluminium tube of 0.8 mm inner diameter. The tip of this tube is located as close as possible to the ion beam. The right position was found by measuring the low-energy electron count rate, with target gas out and comparing it with the dark count level of the detector. We selected the position where we did not observe an electron count-rate over the dark count level. The collision region is located at the focus of a rotatable cylindrical mirror analyser, working with an energy resolution ($R_E = \Delta E_{FWHM}/E$) of 5%. A suppressed Faraday cup collected the outgoing ion beam with the purpose of normalization.

To measure positive ions of low energy (<15 eV), a 1 kV accelerating voltage was applied at the entrance of the electron multiplier detector to increase the detection efficiency. This voltage was applied to the funnel of the detector, covered by a high transmission mesh. In front of the detector there is an aperture that determines a solid angle of detection of 2×10^{-3} sr, also covered with a mesh at ground potential. We have selected this accelerating voltage by noting that there was little increase in detection efficiency on further increasing this voltage, and at the same time dark counts (target gas out) began to increase.

The base pressure in the collision chamber was 7.0×10^{-8} mbar. Measurements were performed at a working pressure of 1.1×10^{-5} mbar with high purity H_2 gas target in. Additionally, we verified that proton spectra showed no variation when the gas target circulated in a chiller, at LN_2 temperature, to condense impurities that could be present in the gas. It is important to note that a large LN_2 trap is present in our collision chamber (Bernardi *et al* 1996), which contributes to ensuring a low contamination level of H_2O (Beckord *et al* 1994).

Typical beam currents were tens of pA for He^{2+} and a few nA for H^+. Background counts with target gas out (at chamber base pressure) were less than 0.1% in the measured spectra.

The proton spectra were measured in the range 0–15 eV at emission angles $\theta = 10°$, 30°, 50°, 70°, 90°, 110°, 130° and 170°. Due to the very low current of the He^{2+} beam, in this case some emission angles ($\theta = 70°$ and 110°) and energies below 3 eV were omitted in the measurements. The effective target thickness dependence on the detection angle was estimated previously (Martínez *et al* 2002). The correction factors applied to the spectra for each emission angle θ are as follows: 0.56 at $\theta = 10°$ and 170°, 0.71 at $\theta = 30°$, 0.89 at $\theta = 50°$ and 130°, 0.97 at $\theta = 70°$ and 110° and 1 at $\theta = 90°$.

In the experimental study of the dependence of the proton yield on the emission angle it is commonly assumed that, due to the small collision time as compared to a typical rotation time of the molecule, the direction of the fragments reproduces the spatial orientation of the internuclear axis at the time of collision. Then, the dependence on the molecular orientation

of the different electronic processes leading to dissociation can be assessed. Experimentally, this kind of measurement requires a detailed knowledge of the 'effective target thickness' as a function of the detection angle, mainly determined by the spatial distribution of the target density and the spectrometer transmission. This problem is particularly cumbersome when yields are smoothly varying with detection angle. In contrast, less severe requirements are needed in the case of electron emission measurements where differential cross sections vary over two orders of magnitude for the complete range of emission angles. Our equipment covers the full angular range, 360°, with the exception of some blind spots (Bernardi *et al* 1996). The possibility to compare spectra measured at positive and negative emission angles (i.e. at both sides with respect to the beam direction) is a sensitive probe for the alignment of beam direction, spectrometer focus and target density distribution. In the case of the present molecular fragmentation measurements, the spectra should also be equivalent for emission angles θ and $\pi - \theta$ for collision systems where momentum transfer from the projectile can be considered as negligible. The reproducibility of the spectra was checked by performing several additional measurements. From these data the uncertainties in the yields have been estimated.

The measured energy distributions of protons $Q(E)$, at each emission angle θ, were divided by the energy E to account for the energy acceptance of the spectrometer ($\Delta E = R_{\mathrm{E}} E$). This procedure allows us to obtain cross section spectra, except for a normalization factor (Bernardi *et al* 1996).

3. Theory and data analysis

Proton production due to H_2 dissociation has contributions from different dissociative states which are populated by electronic transitions induced by the projectile. In accordance with the Franck–Condon principle, the transition probability is determined by the overlap between the initially bound vibrational state of the nuclei and the wavefunction in the continuum. In order to obtain the differential cross sections for proton emission as a function of energy (E), we applied the reflection approximation, which replaces the continuum wavefunction by a suitable δ function (Coolidge *et al* 1936, Yousif *et al* 1988). The potential energy curves involved in calculations, shown in figure 1(a), were those given by Sharp (1971). As a further approximation, the ground state of the harmonic oscillator was used instead of the initial vibrational state of H_2.

The analysis of experimental results requires that the translational thermal motion of the target molecules be considered. Therefore, the predicted energy distributions of the emitted protons were broadened by taking into account a Maxwell–Boltzmann distribution for the gas target (Chantry and Schulz 1967). This effect contributes about 10–15% to the FWHM of the calculated distributions, shown in figure 1(b).

In order to discuss the experimental results we applied a fitting procedure to the proton energy spectra, for each emission angle θ, using the four repulsive states: $2p\pi_u$, $2s\sigma_g$, $2p\sigma_u$ and CE (H^+H^+). The yields obtained for each of these contributions allow us to obtain differential cross sections as a function of the emission angle. By integrating these data we also get the total cross section corresponding to each state.

In the case of fragmentation induced by He^{2+} projectiles, particularly at 25 and 50 keV amu^{-1}, we obtained small, but systematic, disagreements between the fitting curve and the experimental spectra in the energy range of the faster protons. Although an energy shift of the order of 0.1 eV or less is observed in the high energy tail of the spectra, it could lead to a mistaken estimation of the yields of the CE and the nearby $2p\sigma_u$ channels. Taking into account that, at these projectile energies, double capture and transfer ionization are much more likely than double ionization, we decided to quantify the effect of the momentum transfer

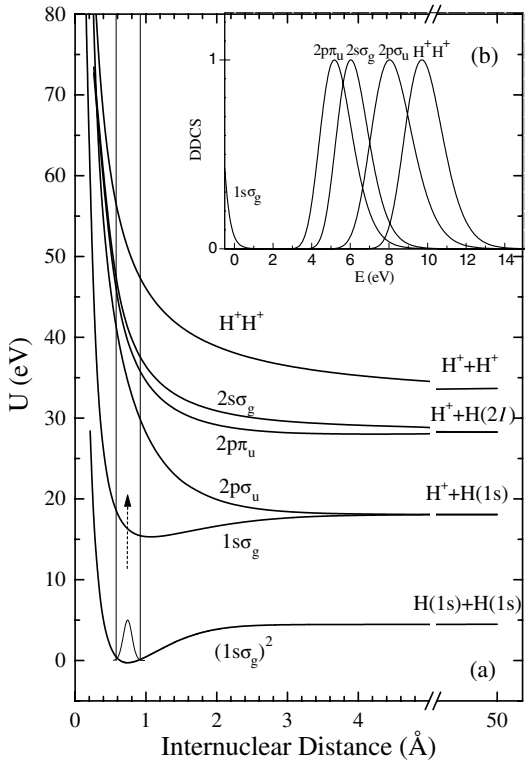

Figure 1. (a) Potential energy curves for selected states of H_2, H_2^+ and H_2^{2+} (Sharp 1971). (b) Predicted fragment energy distributions based on the Franck–Condon model and corresponding to the states in (b).

to the target in capture processes. For this purpose we applied a model similar to that used by Frémont *et al* (2000) and Adoui *et al* (2001) for double capture by O^{5+} on H_2, where the n-body problem is treated as two successive two-body problems. The validity of this two-step mechanism was established for a wide range of the ratio between the projectile charge and the incident velocity, $Z/v_P \lesssim 100$ (Ali *et al* 2001). Basically, the electronic process takes place in a first step, then fragmentation occurs in an isolated way as a second step.

The momentum transfer to the centre of mass (CM) of the recoiling target, $\boldsymbol{K}_r$, can be evaluated using the momentum and energy conservation equations as a function of the projectile deflection angle. In order to estimate the deflection angles we used the overbarrier model (Niehaus 1986) and the classical Rutherford scattering calculations for small angles (Guillemot *et al* 1990). In particular, the longitudinal component with respect to the incident projectile direction, $K_{r\|}$, almost equals the values obtained with the conservation equations in an approximation where the longitudinal and transversal components are uncoupled:

$$K_{r\|}^{DC} \simeq \frac{Q}{v_P} - v_P \tag{1}$$

$$K_{r\|}^{TI} \simeq \frac{Q - T_{el}}{v_P} - \frac{v_P}{2} + k_{el} \tag{2}$$

where Q is the difference between the final and initial binding electron energies and $T_{el} = \frac{1}{2}k_{el}^2$ is the electron energy in the continuum. Finally, the doubly differential cross section for proton

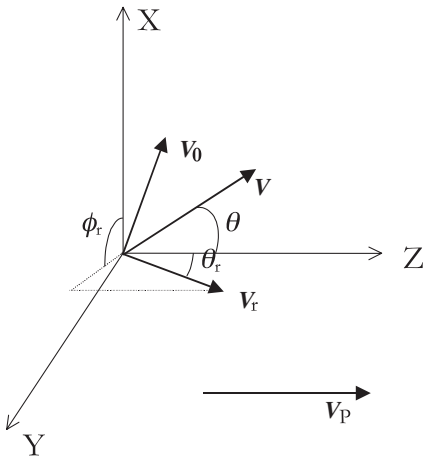

Figure 2. Kinematic parameters for the two-step collision–fragmentation process. The angles θ, θ_r and ϕ_r refer to the emission angle of the proton in the laboratory frame, the polar and azimuth angles of the recoil, $\boldsymbol{K}_r = 2M_p\boldsymbol{v}_r$, respectively. $\boldsymbol{v}$ and $\boldsymbol{v}_0$ refer to the proton velocity in the laboratory frame and the molecular CM frame, respectively. $\boldsymbol{v}_P$ is the projectile velocity and the XZ plane is the detection plane.

emission by CE was obtained in the laboratory frame by the transformation

$$\left(\frac{d^2\sigma}{dE\,d\Omega}\right)_{Lab} = \left(\frac{E}{E_0}\right)^{1/2}\left(\frac{d^2\sigma}{dE_0\,d\Omega_0}\right)_{CM} \tag{3}$$

$$E_0 = E + E_r - 2(E\,E_r)^{1/2}(\sin\theta\sin\phi_r\cos\theta_r + \cos\theta\cos\phi_r) \tag{4}$$

where the double differential cross section in the CM frame is as shown in figure 1(b). Here, $E = \boldsymbol{K}^2/2M_p$ and θ are the energy and emission angle of the proton in the laboratory frame, $E_0 = \boldsymbol{K}_0^2/2M_p$ is the proton energy in the CM frame and $E_r = \boldsymbol{K}_r^2/8M_p$. The polar ($\theta_r$) and azimuth ($\phi_r$) angles of $\boldsymbol{K}_r$ are shown in figure 2. To obtain the differential cross sections, we performed an integration in ϕ_r. θ_r is related to the deflection angle of the projectile, which is estimated for each process.

From the fitting procedure of the spectra for each emission angle, uncertainties in the contributions of each one of the dissociative states were estimated. Typical values were 3%, for CE and $2p\sigma_u$ states, and between 8 and 50%, for $2s\sigma_g$ and $2p\pi_u$. The larger uncertainties were obtained for He^{2+} projectiles, particularly at 25 keV amu^{-1}. The uncertainty in the calibration of the energy axis was also included in this estimation.

4. Results and discussion

4.1. Energy distribution of fragments

We present here the energy distributions of protons and discuss the results of a fitting procedure using four repulsive states: $2p\pi_u$, $2s\sigma_g$, $2p\sigma_u$ and CE. The measured spectra for H^+ and He^{2+} projectiles at 25, 50 and 100 keV amu^{-1} are shown in figures 3–5 for laboratory emission angles $\theta = 10°, 50°$ and $90°$. Present measurements, the contribution of individual dissociation channels and the resulting total spectra are also displayed in the figures.

For the H^+ ion impact case, it can be seen that the fitted spectra show good agreement with data, except for proton energies below 4 eV. The disagreement is larger for the collision energies

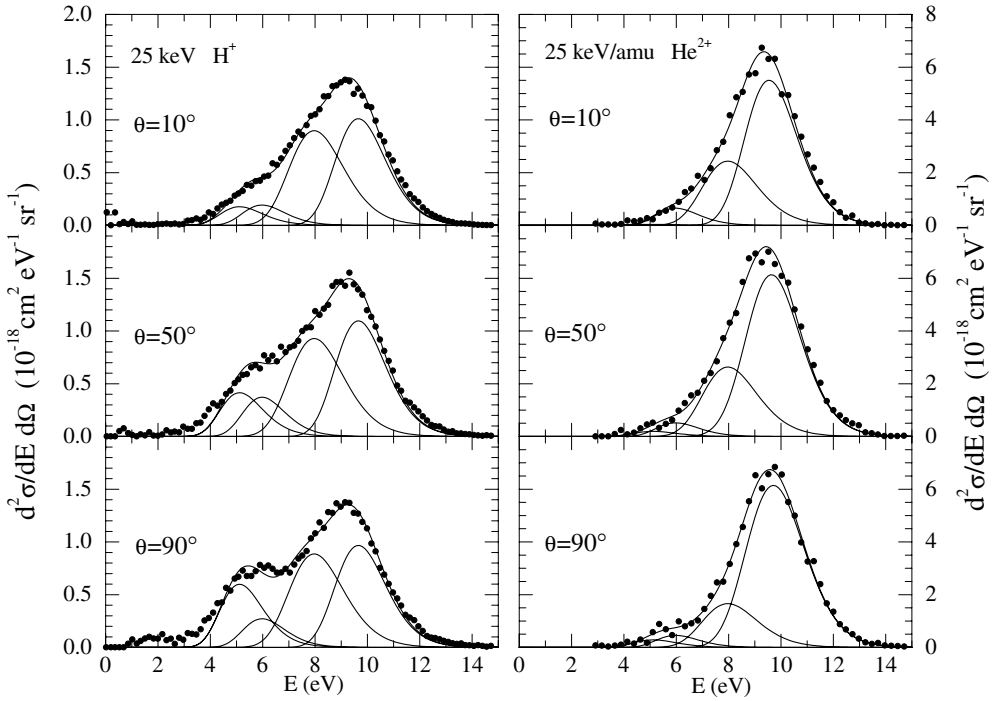

Figure 3. Double differential cross sections for 25 keV amu^{-1} H^+ (left) and He^{2+} (right) on H_2. ●, present data; ——, fitting curves for the four dissociative states considered and the sum of them. The proton emission angles are, from top to bottom, $\theta = 10°$, 50° and 90°.

25 and 50 keV and increases towards 90°. Additional low energy contributions, not included in the four states considered, may result from AI processes, as mentioned in the introduction. AI is a well-known proton emission mechanism, observed, for example, by Edwards *et al* (1990) above 350 keV for H^+ impact, though at the present impact energies only a small contribution is expected. The fact that the data show an increase of the contribution towards 90° suggests that the population of AI states has a dependence on the molecular orientation. The larger variation of the individual yields with the emission angle is observed for the $2p\pi_u$ state, though the overlap with the low energy contribution should also be considered. Measurements for 5–25 keV H^+ on H_2 by Lindsay *et al* (1987) also show an orientation dependence of the yield for the $2p\pi_u$ contribution, with a maximum at 90°.

For the collision system He^{2+} on H_2, energy spectra of the protons were not previously reported by other laboratories. To obtain a better agreement with the measured spectra for proton energies ∼7–15 eV, we found it appropriate for He^{2+} impact to include the effect of the momentum transfer to the target in the calculated CE contribution. Following the procedure outlined in section 3, the momentum transfer is evaluated for two-electron processes leading to CE. In order to obtain the final CE distribution in the laboratory frame to fit the spectra, the momentum transfer for each process is weighted with the total cross section values shown in table 1. However, to obtain a first approach we simplified calculations by disregarding the momentum transfer in DI: therefore only DC and TI were taken into account. We used the ionization potential of H_2 given by Hoekstra *et al* (1994). It is assumed that He(1s2s) is the preferred final state in DC (Juhász *et al* 2002, Errea *et al* 2003), although only impact energies up to 20 keV amu^{-1} were considered in these references. At 50 and 100 keV amu^{-1} projectile

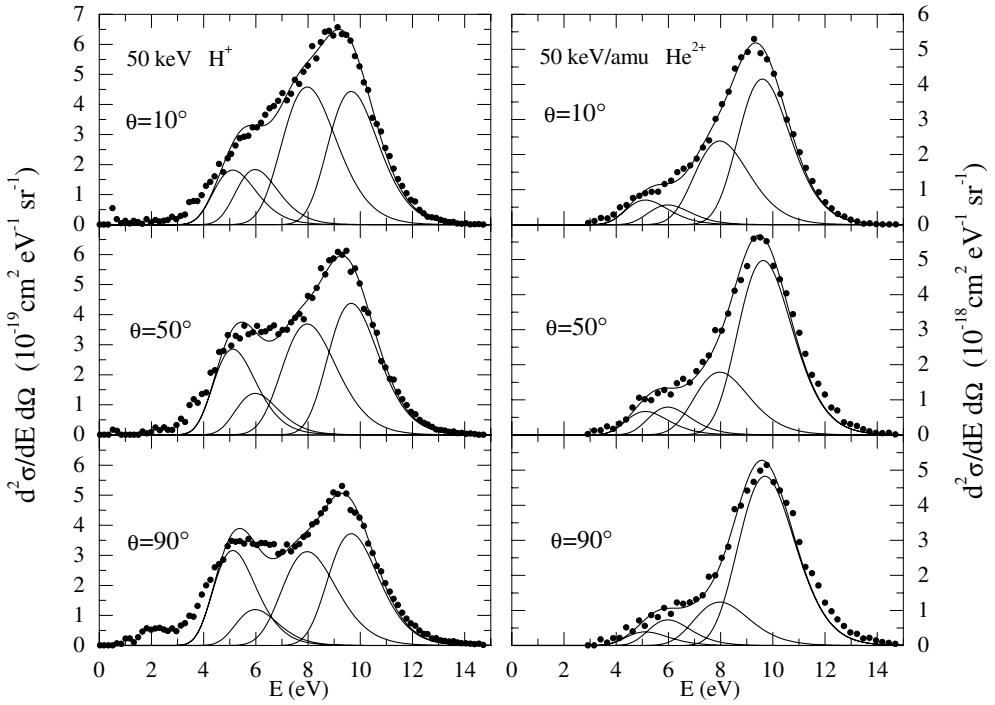

Figure 4. Same as in figure 3 for 50 keV amu^{-1}.

Table 1. Previously measured total cross sections for H^+ and He^{2+} ion beams incident on a H_2 target. TI, transfer ionization; DC, double capture; DI, double ionization; CE, Coulomb explosion ($\sigma_{CE} = \sigma_{TI}+\sigma_{DC}+\sigma_{DI}$); D-CAP, dissociative capture (including TI); D-ION, dissociative ionization (including TI); σ_d, total dissociation ($\sigma_d = \sigma_{D-CAP} + \sigma_{D-ION} - \sigma_{TI}$).

Incident ion	Energy (keV amu^{-1})	Cross sections (10^{-16} cm^2)						
		TI	DC	DI	CE	D-CAP	D-ION	σ_d
He^{2+}	25	1.09[a]	0.60[c]	0.032[d]	1.72	1.90[a]	1.33[a]	2.15
	50	0.9[a]	0.29[c]	0.06[d]	1.25	1.62[a]	1.54[a]	2.25
	100	0.24[b]	0.04[c]	0.12[e]	0.40	—	1.06[b]	—
H^+	25	0.2345[a]	0.072 3[f]	—	0.307	0.70[a]	0.335[a]	0.80
	50	0.077[a]	0.016[f]	—	0.12	0.22[a]	0.251[a]	0.394
	100	0.0107[a]	0.000 315[f]	0.003 96[g]	0.015	—	0.146[b]	—

[a] Shah *et al* (1989).
[b] Shah and Gilbody (1982).
[c] Shah and Gilbody (1978).
[d] Afrosimov *et al* (1980).
[e] Extrapolated from Edwards *et al* (1990).
[f] Barnett (1990).
[g] Edwards *et al* (1985).

energies, minor differences were found by considering either the He(1s2p) or the He($1s^2$) final states and, as the cross section for DC decreases with increasing impact velocity, the estimated momentum transfer does not strongly depend on the capture final state. We considered He^+(2p) the most likely final state of the projectile in TI (Afrosimov *et al* 1980, Meng *et al* 1994). The

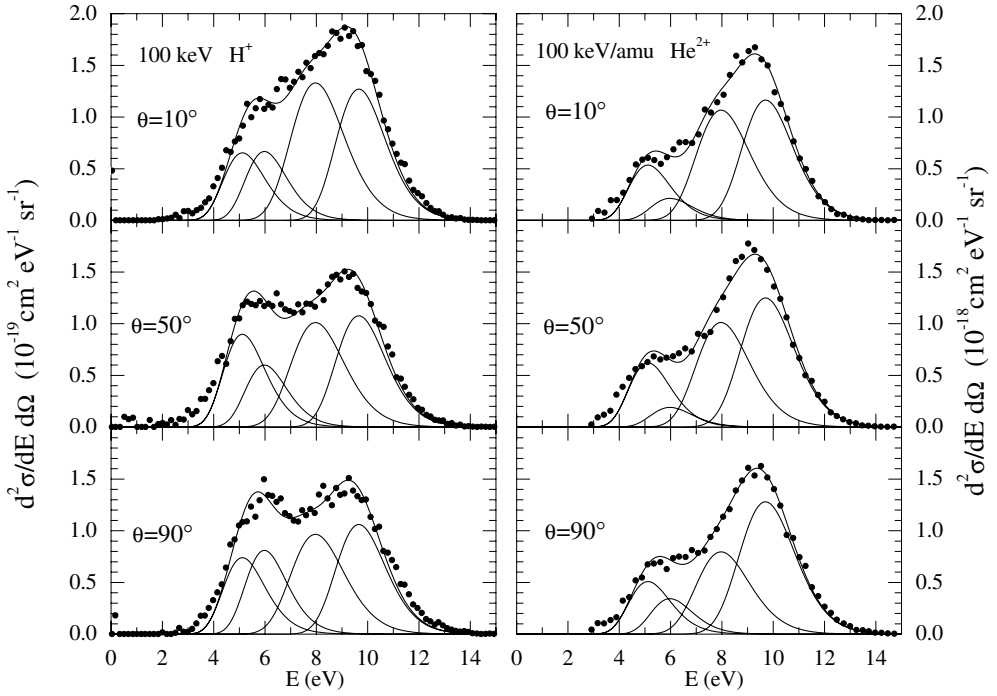

Figure 5. Same as in figure 3 for 100 keV amu^{-1}.

estimated momentum transfer and recoil angle for He^{2+} impact are: $K_r^{DC} = 4.4$ au, $\theta_r = 115°$, $K_r^{TI} = 1.8$ au, $\theta_r = 81°$ at 25 keV amu^{-1}; $K_r^{DC} = 3.1$ au, $\theta_r = 131°$, $K_r^{TI} = 2.4$ au, $\theta_r = 97°$ at 50 keV amu^{-1}; and $K_r^{DC} = 3.8$ au, $\theta_r = 130°$, $K_r^{TI} = 3.0$ au, $\theta_r = 102°$ at 100 keV amu^{-1}. In figure 6 we present a comparison, using the spectrum at $\theta = 90°$ for 25 keV amu^{-1} He^{2+} impact, to show that a more accurate fit to the data is achieved by including the momentum transfer in the collision (figure 6(b)). The effect of momentum transfer was clearly observed in dissociation by highly charged and low velocity projectile impact (Adoui *et al* 2001, Ali *et al* 2001). However, the present measurements are also sensitive to it.

The spectra for He^{2+} (figures 3–5) are markedly different as compared to those for H^+ impact. The contributions of $2p\sigma_u$ and CE channels dominate the spectra, while the $2p\pi_u$ and $2s\sigma_g$ yields rise as the incident energy increases from 25 to 100 keV amu^{-1}. This behaviour can be understood from total cross section data, summarized in table 1. The cross section values for CE (σ_{CE}) were estimated by adding DC, TI and DI total cross sections, while the dissociation cross section (σ_d) includes all dissociation channels producing protons. Comparing σ_{CE} and σ_d at 25 and 50 keV amu^{-1} impact, we found that CE represents a large contribution, with more than 50%. At these impact energies TI and DC are more likely than other dissociative processes and lead to CE. At 100 keV amu^{-1} the CE contribution decreases below 40% as the cross sections for TI and DC decrease too.

4.2. Angular cross sections

We have obtained differential cross sections for proton production, as a function of emission angle θ, for the dissociation channels considered above. To this purpose, we integrated in energy the different contributions, considering the weight factors as they resulted from the

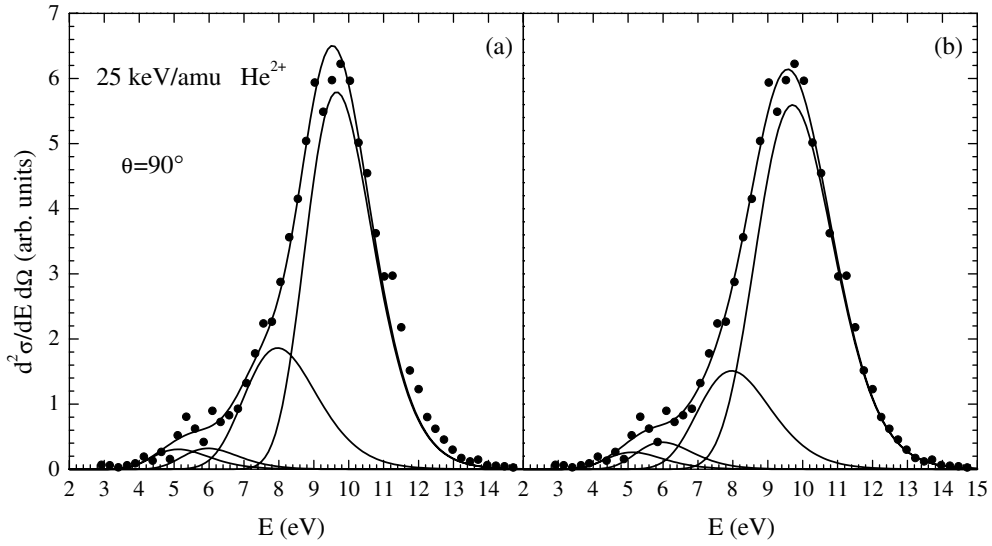

Figure 6. The fits to data derived from (a) the Franck–Condon model and (b) by applying equation (3) to the CE channel. Recoil momentum correction for the spectrum measured at $\theta = 90°$ and for He^{2+} on H_2 at 25 keV amu^{-1}.

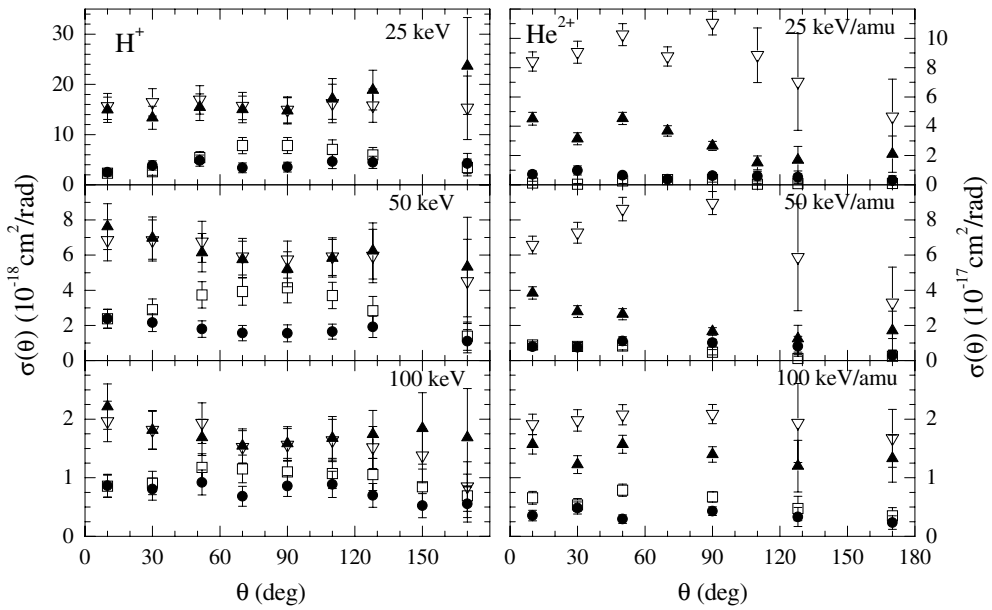

Figure 7. Angular cross sections of secondary protons arising from $2p\pi_u$ (□), $2s\sigma_g$ (●), $2p\sigma_u$ (▲) and H^+H^+ (▽) repulsive states of the hydrogen molecular ions. Left panel: H^+ on H_2 at 25, 50 and 100 keV (from top to bottom). Right panel: He^{2+} on H_2 at 25, 50 and 100 keV amu^{-1} (from top to bottom).

fit of the measured energy spectra. The results for H^+ and He^{2+} at the three measured incident energies are shown in figure 7. Error bars are mainly due to the uncertainties in the relative yields of the energy spectra measured at different emission angles, but also include

Table 2. Obtained total cross sections; σ_d, total dissociation cross section (all channels).

Incident ion	Energy (keV amu^{-1})	Cross sections (10^{-17} cm^2)				
		$2p\pi_u$	$2s\sigma_g$	$2p\sigma_u$	H^+H^+	σ_d
He^{2+}	25	0.38 ± 0.24	1.12 ± 0.55	5.33 ± 1.03	17.24 ± 2.96[a]	24.08 ± 5.52
	50	0.90 ± 0.37	1.76 ± 0.61	3.58 ± 0.83	14.47 ± 2.64	20.71 ± 5.02
	100	1.17 ± 0.25	0.70 ± 0.20	2.59 ± 0.45	3.83 ± 0.62	8.28 ± 1.77
H^+	25	1.21 ± 0.29	0.79 ± 0.22	3.16 ± 0.65	3.07 ± 0.61[a]	8.24 ± 2.14
	50	0.67 ± 0.15	0.34 ± 0.10	1.15 ± 0.24	1.17 ± 0.24	3.34 ± 0.91
	100	0.20 ± 0.05	0.15 ± 0.04	0.33 ± 0.07	0.31 ± 0.07	0.99 ± 0.28

[a] Previously measured values (for authors see table 1).

the uncertainties for each contribution derived from the fitting procedure. Absolute cross section values were obtained from the normalization of data to the total cross section values, as explained in the next section.

In the case of He^{2+} incidence, a forward–backward asymmetry, emission angles θ and $\pi - \theta$, is expected in the angular cross sections due to momentum transfer to the target in the collision. However, a small asymmetry is also observed for H^+ impact, for which no indication of momentum transfer could be detected in the energy spectra. We conclude that, due to the uncertainties in the spectra, particularly at large angles, $\theta > 90°$, we cannot obtain information about momentum transfer from the present angular distributions. In order to compare with data obtained in other laboratories, we applied the same analysis as Lindsay *et al* (1987) to the case of H^+ impact at 25 keV, also measured by these authors. They expand the differential cross section as $\sigma(\theta) = \frac{\sigma}{4\pi}[1 + \beta P_2(\cos\theta)]$, where σ is the total cross section, $P_2(\cos\theta) = \frac{1}{2}(3\cos^2\theta - 1)$ is a Legendre polynomial and β is the anisotropy parameter. We obtained the following values for the β parameter: $2p\pi_u$, -0.62 (-0.50); $2s\sigma_g$, -0.09 (-0.12); $2p\sigma_u$, 0.11 (0.22) and CE, 0.00 (0.09), where the values in parentheses are from Lindsay *et al* (1987). Within uncertainties, good agreement for the anisotropy parameter is found. The $2p\pi_u$ contribution shows a clear angular dependence, also present for 50 and 100 keV incident energies. The remaining dissociation channels show slight anisotropy.

4.3. Total cross sections

Total cross sections were obtained by integrating the angular cross sections. In order to get absolute cross section values, we normalized the CE channel at 25 keV amu^{-1}, for H^+ and He^{2+}, to the σ_{CE} values in table 1, obtained from DC, TI and DI cross sections (Shah *et al* 1989). Then, all other absolute cross sections are obtained from the relative normalization of the data by using the same factors. These results are shown in table 2 and figure 8. We included also the values of the total dissociation cross sections, σ_d, as obtained from the present data by adding the four dissociation channels. A satisfactory agreement is observed with the values of σ_d from table 1, obtained from dissociation cross section measurements previously reported. However, differences can be attributed to GSD producing low energy protons that are not included in our data. The proton production by GSD was estimated as 1.5% of the H_2^+ production (Ben-Itzhak *et al* 1996). Using this result, we estimated a contribution of GSD in total dissociation (σ_d) in the range 10–20% for H^+ and 6–7.5% for He^{2+}, at our collision energies, with larger contributions as the impact energy increases.

Comparison with previous estimates of cross sections for each dissociative state is possible for 25 keV H^+ projectiles from measurements by Lindsay *et al* (1987). Although good

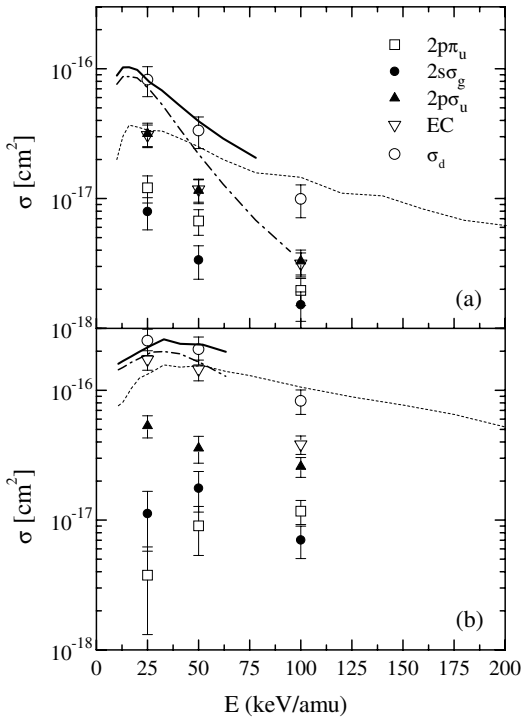

Figure 8. Total cross sections of dissociative processes in H^+ (a) and He^{2+} (b) on H_2. Present results: □, $2p\pi_u$; ●, $2s\sigma_g$; ▲, $2p\sigma_u$; ▽, H^+H^+; ○, σ_d, as explained in the text. Results from Shah and Gilbody (1982) and Shah *et al* (1989) for: - - - -, dissociative ionization; — · —, dissociative capture; ——, sum of dissociative processes.

agreement is obtained for the CE channel, the cross section for the $2p\sigma_u$ state is a factor of 2 over our value, while for the $2p\pi_u$ and $2s\sigma_g$ states they obtained cross section values 50% higher than ours. It must be noted that Lindsay *et al* used a different set of data for normalization to get absolute cross section values.

The dependence of the cross sections with the projectile charge for different dissociation channels can be discussed from the ratio of the values obtained from He^{2+} and H^+ impact. Two-electron processes leading to CE (DC, TI and DI) and other dissociation channels (capture or ionization plus excitation) are complex many-body problems and not easy to discuss from the present experimental data. Even in an independent electron approximation, for one-electron capture, ionization or excitation processes, it is difficult to predict the dependence on the projectile charge in the present incident energy range. At the lowest impact energy, the validity of the quasi-molecular collision treatment is exceeded and at the highest energy the collision is below the perturbative regime, though it is interesting to observe the increment of fragment production when the projectile doubles its charge. From the total cross section data in table 2, the ratio of double to single charge for CE resulted in: 5.6, 12.4 and 12.3 at 25, 50 and 100 keV amu^{-1}, respectively. Viewed as a scaling, the values are comprised within Z^2 and Z^4. Considering the other channels by adding the total cross sections for the $2p\pi_u$, $2s\sigma_g$ and $2p\sigma_u$ states, the ratios, smaller than for CE, are: 1.3, 2.9 and 6.6 for 25, 50 and 100 keV amu^{-1}, respectively.

5. Conclusions

We have investigated proton production in H_2 dissociation by H^+ and He^{2+} ion impact at intermediate energies. The energy spectra of protons are well described by a model based on the Franck–Condon principle considering the CE channel and three excited states of H_2^+ induced by collision: $2p\pi_u$, $2s\sigma_g$ and $2p\sigma_u$. We observed some disagreement in the low energy region of the spectra for H^+ impact that could be attributed to a contribution from AI of doubly excited states of H_2. In the case of He^{2+} projectiles, it was found that the momentum transfer to the target must be considered in order to account for the shape of the energy spectra. This effect was included in the model for the CE channel by means of a two-step calculation, using the momentum–energy conservation equations and simple estimates for the deflection angle of the projectile. When the spectra for He^{2+} are compared to those for H^+ projectiles, the main effect observed is the enhancement of capture in two-electron processes, by means of double capture and transfer ionization.

The energy spectra, covering the full range of proton emission angles, allow us to obtain angular cross sections as well as total cross sections for the dissociation channels proposed in the model. Although the large uncertainties in the angular cross sections and some asymmetry are attributed to effective target thickness variations, measured anisotropy parameters for 25 keV H^+ impact are in good agreement with previous measurements (Lindsay *et al* 1987). Total cross sections for dissociation, obtained by integration of our differential cross sections, are in agreement with previous total cross section measurements. Contributions from low energy protons due to GSD, not included in our data, should be considered in order to get a better comparison. Theoretical calculations, dealing with the difficulties of a many-body problem at intermediate impact energy, would be of great interest for a better understanding of the many features found in the present and previous work.

Acknowledgments

Support from the Consejo Nacional de Investigaciones Científicas y Técnicas, the Agencia Nacional de Promoción Científica y Técnica (Contrato de Préstamo BID 1201/OC-AR, grant no 03-04021) and Fundación Antorchas is gratefully acknowledged.

References

Adoui L, Tarisien M, Rangama J, Sobocinsky P, Cassimi A, Chesnel J-Y, Frémont F, Gervais B, Dubois A, Krishnamurty M, Kumar S and Mathur D 2001 *Phys. Scr.* T **92** 89

Afrosimov V V, Leiko P A and Panov M N 1980 *Sov. Phys.—Tech. Phys.* **25** 313

Ali I, Dörner R, Jagutzki O, Nüttgens S, Mergel V, Spielberger L, Khayyat Kh, Vogt T, Bräuning H, Ullmann K, Moshammer R, Ullrich J, Hagmann S, Groeneveld K, Cocke C L and Schmidt-Böcking H 1999 *Nucl. Instrum. Methods* B **149** 490

Ali I, DuBois R D, Cocke C L, Hagmann S, Feeler C R and Olson R E 2001 *Phys. Rev.* A **64** 022712

Barnett C F 1990 *Atomic Data For Fusion* vol 1 (Oak Ridge, TN: Oak Ridge National Laboratory) ORNL-6086, A30

Beckord K, Becker J, Werner U and Lutz H O 1994 *J. Phys. B: At. Mol. Opt. Phys.* **27** L585

Ben-Itzhak I, Krishnamurthi V, Carnes K D, Aliabadi H, Knudsen H, Mikkelsen U and Esry B D 1996 *J. Phys. B: At. Mol. Opt. Phys.* **29** L21

Bernardi G, Suárez S, Fregenal D, Focke P and Meckbach W 1996 *Rev. Sci. Instrum.* **67** 1761

Burrows M D, McIntyre L C, Ryan S R and Lamb W E 1980 *Phys. Rev.* A **21** 1841

Chantry P J and Schulz G J 1967 *Phys. Rev.* **156** 134

Coolidge A S, James H M and Present R D 1936 *J. Chem. Phys.* **4** 193

Dörner R, Mergel V, Jagutzki O, Spielberger L, Ullrich J, Moshammer R and Schmidt-Böcking H 2000 *Phys. Rep.* **330** 96

Dunn G H and Kieffer L J 1963 *Phys. Rev.* **132** 2109

Edwards A K, Wood R M and Ezell R L 1985 *Phys. Rev.* A **31** 99
Edwards A K, Wood R M and Ezell R L 1990 *Phys. Rev.* A **42** 1799
Edwards A K, Wood R M, Mangan M A and Ezell R L 1992 *Phys. Rev.* A **46** 6970
Errea L F, Macías A, Méndez L, Pons B and Riera A 2003 *J. Phys. B: At. Mol. Opt. Phys.* **36** L135
Frémont F, Bedouet C, Tarisien M, Adoui L, Cassimi A, Dubois A, Chesnel J-Y and Husson X 2000 *J. Phys. B: At. Mol. Opt. Phys.* **33** L249
Guillemot L, Roncin P, Gaboriaud M N, Laurent H and Barat M 1990 *J. Phys. B: At. Mol. Opt. Phys.* **23** 4293
Hoekstra R, Folkerts H O, Beijers J P M, Morgenstern R and de Heer F J 1994 *J. Phys. B: At. Mol. Opt. Phys.* **27** 2021
Ito K, Hall R I and Ukai M 1996 *J. Chem. Phys.* **104** 8449
Juhász Z, Lubinski G, Morgenstern R and Hoekstra R 2002 *At. Plasma-Mater. Interaction Data Fusion* **10** 25
Köllman K 1978 *J. Phys. B: At. Mol. Phys.* **11** 339
Landau M, Hall R I and Pichou F 1981 *J. Phys. B: At. Mol. Phys.* **14** 1509
Latimer C J 1993 *Adv. At. Mol. Opt. Phys.* **30** 105
Latimer C J, Dunn K F, Kouchi N, McDonald M A, Srigengan V and Geddes J 1993 *J. Phys. B: At. Mol. Opt. Phys.* **26** L595
Lindsay B G, Yousif F B, Simpson F R and Latimer C J 1987 *J. Phys. B: At. Mol. Phys.* **20** 2759
Martínez S, Bernardi G, Focke P, González A D and Suárez S 2002 *J. Phys. B: At. Mol. Opt. Phys.* **35** 2261
Meng L, Olson R E, Folkerts H O and Hoekstra R 1994 *J. Phys. B: At. Mol. Opt. Phys.* **27** 2269
Niehaus A 1986 *J. Phys. B: At. Mol. Phys.* **19** 2925
Sánchez I and Martín F 1999 *Phys. Rev.* A **60** 2200
Savage O G, Lindsay B G and Latimer C J 1990 *J. Phys. B: At. Mol. Opt. Phys.* **23** 4313
Shah M B and Gilbody H B 1978 *J. Phys. B: At. Mol. Phys.* **11** 121
Shah M B and Gilbody H B 1982 *J. Phys. B: At. Mol. Phys.* **15** 3441
Shah M B, McCallion P and Gilbody H B 1989 *J. Phys. B: At. Mol. Opt. Phys.* **22** 3037
Sharp T E 1971 *At. Data* **2** 119
Strathdee S and Browning R 1979 *J. Phys. B: At. Mol. Phys.* **12** 1789
Wolff W, Ben-Itzhak I, Wolf H E, Cocke C L, Abdallah M A and Stöckli M 2002 *Phys. Rev.* A **65** 042710
Wood R M, Edwards A K and Steuer M F 1977 *Phys. Rev.* A **15** 1433
Yousif F B, Lindsay B G and Latimer C J 1988 *J. Phys. B: At. Mol. Opt. Phys.* **21** 4157
Zare R N 1967 *J. Chem. Phys.* **47** 204